Single-Walled Carbon Nanotubes Probing the Denaturation of Lysozyme

Liming Xie,[†,‡] Shin G. Chou,[*,§,∥] Ajay Pande,[⊥] Jayanti Pande,[⊥] Jin Zhang,[*,†] Mildred S. Dresselhaus,[†,#] Jing Kong,[*,†] and Zhongfan Liu[†]

Department of Electrical Engineering and Computer Science, Massachusetts Institute of Technology, Cambridge, Massachusetts 02139, Beijing National Laboratory for Molecular Sciences, College of Chemistry and Molecular Engineering, Peking University, Beijing 100871, P. R. China, Pfizer Global Research and Development, Pfizer Inc., Groton, Connecticut 06340, Optical Technology Division, National Institute of Standards and Technology, Gaithersburg, Maryland 20899, Chemistry Department, University at Albany, State University of New York, Albany, New York 12222, and Department of Physics, Massachusetts Institute of Technology, Cambridge, Massachusetts 02139

Received: December 24, 2009; Revised Manuscript Received: March 2, 2010

Resonance Raman spectroscopy measurements of lysozyme-bound single-walled carbon nanotubes have been made during different stages of the chemically and thermally induced misfolding and of the denaturation process of nanotube-bound lysozymes. Changes to the Raman intensity of single-walled carbon nanotubes (SWNTs) have been observed during the denaturation of lysozyme. The Raman intensity changes are attributed to excitonic transition energy (E_{ii}) shifts of the SWNTs during the denaturation of lysozyme. The E_{ii} shift of SWNTs was confirmed by photoluminescence measurements.

Introduction

Irreversible degradation and aggregation of therapeutic proteins is a long-standing problem in the biopharmaceutical industry. To ensure product integrity at the time of administration, a high concentration protein product must remain stable for an extended period of time during transport and storage, often at elevated temperatures.[1] The degradation process is generally described as a multistage pathway, starting with the unfolding and misfolding in protein monomers and the onset of protein degradation and aggregation, involving a complex set of competing misfolding and self-association reactions. In this manner, a fraction of the overall product may be degraded, and the small percentage of degradation can sometimes be laborious and time-consuming to detect and resolve using chromatography and light-scattering methods. Recent developments in self-interaction nanoparticle spectroscopy[2] using gold nanoparticles suggest that the very sensitive optical transitions of nanoparticles could be exploited to develop a nanoparticle-based protein interaction assay to readily detect changes in the weak protein−protein versus protein−nanoparticle interactions in misfolded protein products. Aside from gold nanoparticles, one of the particularly interesting candidates for such nanoscaled probes is single-walled carbon nanotubes (SWNTs).

SWNTs have unique electronic properties and rich spectroscopic properties.[3,4] The detailed geometric structure of SWNTs as denoted by their (n,m) indices determines their electronic properties[5,6] as well as their spectroscopic properties, and these subjects have been studied extensively. Because the excitonic transition energy (E_{ii}) of SWNTs is particularly sensitive to the dielectric environment,[7,8] SWNTs have been used in a number of optical and electrical devices to directly probe conformational changes in biomacromolecules. The strong and photobleach-resistant photoluminescence (PL) and resonance Raman signals in the near-infrared region makes SWNTs promising as labels in biosystems.[9,10] For example, the shift of the PL emission energy of DNA-wrapped SWNTs due to the wrapping agent has been used to monitor conformational changes in DNA.[11,12] In this report, we use optical spectroscopy to qualitatively probe the interactions in a complex system involving a small percentage of misfolded/denatured proteins and nanotubes. Even though the weak interactions between a nanotube and a fraction of the degraded proteins can cause a small, yet definitive, shift in E_{ii}, the shift in the PL signal could be difficult to resolve with high-energy resolution due to the wide resonance window of SWNTs in a biological environment. Thus, resonance Raman spectroscopy was used as an additional (yet possibly more sensitive) probe to detect subtle shifts in the position of the resonance window and the position of the E_{ii}[13−15] as a result of the altered protein−nanotube and protein−protein interactions, when a small fraction of the proteins in the solution undergo denaturation.

Many proteins can be attached to SWNTs through noncovalent binding.[16,17] In this study, lysozyme was chosen as a model protein to study the protein−nanotube interaction. With 129 residues, lysozyme is a small and widely studied model protein whose folding kinetics is well-understood. In its native state, 83% of the surface of the lysozyme is hydrophobic,[18] with a hydrophobic box defined by residues Trp 28, Trp 111, Tyr 23, Met 105, and Trp 108,[19−21] and the stability and weak interactions are mostly determined by the colloidal stability of the proteins in solution. As we initiate misfolding and denaturation reactions, the secondary structure and the hydrophobic interior region of lysozyme are gradually exposed, and eventually, the protein is unfolded.

For the lysozyme-wrapped SWNTs (LYZ-SWNTs) without any denaturant, SWNTs may be bound to the hydrophobic

* To whom correspondence should be addressed. Tel: 1-617-519-5475 (S.G.C.), 1-617-324-4068 (J.K.). E-mail: sgchou@nist.gov (S.G.C.), jingkong@mit.edu (J.K.), jinzhang@pku.edu.cn (J.Z.).
† Department of Electrical Engineering and Computer Science, Massachusetts Institute of Technology.
‡ Peking University.
§ Pfizer Inc.
∥ National Institute of Standards and Technology.
⊥ State University of New York in Albany.
Department of Physics, Massachusetts Institute of Technology.

10.1021/jp9121497
Published on Web 04/02/2010

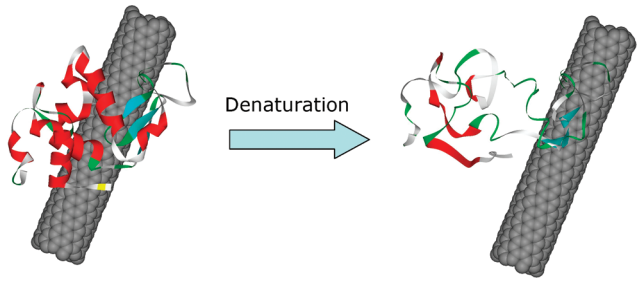

Figure 1. Schematic illustration of structures of a lysozyme-wrapped SWNT and a denatured lysozyme-wrapped SWNT.

pocket of lysozyme through hydrophobic interactions and $\pi-\pi$ stacking.[16] Circular dichroism (CD) spectra have shown that the secondary and tertiary structures of the lysozyme are preserved in the native state in the LYZ-SWNT[16] complex. During the denaturation process, the secondary and tertiary structures of the protein are significantly disturbed. As a result, more solvent molecules surround the SWNTs. Figure 1 shows a schematic illustration of structures of LYZ-SWNT before and after lysozyme denaturation (they are not the real structures). As shown in Figure 1, the expected change in the lysozyme−SWNT binding geometry effectively changes the dielectric surroundings of SWNTs, which can shift the E_{ii}[7,8] and then change the PL and Raman spectra of the SWNTs. In this report, we measured the Raman spectra of SWNTs in a LYZ-SWNT dispersion during the misfolding and denaturation of the lysozyme by either adding guanidinium hydrochloride or heating.

Experiments

The adsorption of lysozyme and the creation of a LYZ-SWNT dispersion was achieved by the sonication of 0.3% CoMoCAT SWNTs in a 5−10 mg/mL lysozyme (Aldrich-Sigma) solution for 30 min, followed by centrifugation at 11 000*g* for 1 h. Two methods were used to introduce lysozyme misfolding and denaturation. One was chemical denaturation and the other was thermal denaturation. Different concentrations of guanidinium hydrochloride (GndHCl, Aldrich-Sigma) were used to chemically induce denaturation of the lysozyme molecules, and the solution pH was maintained by using 5 mM of acetate buffer (pH = 5.0). After incubation, circular dichroism (CD) spectroscopy, Raman, and PL were measured for the LYZ-SWNT dispersion at different GndHCl concentrations. For the thermal denaturation, a LYZ-SWNT dispersion was injected into a tube in a hot-water bath at different temperatures. At different time intervals during the denaturation process, a small volume of solution for spectral characterization was withdrawn and cooled down using a cold-water bath. The CD was measured by a J815 model JASCO CD spectrometer in a 1 mm path length cuvette. For Raman measurements, a Kr-ion laser (647 nm) and a Nd:YAG laser (532 nm) were used to excite the SWNTs, and a 10× objective was used to focus the excitation laser and to collect the Raman signal. A typical integration time for taking a Raman spectrum is 10 s with five accumulations. The PL measurement was conducted in a home-built setup: a 658 nm diode laser, a 50× aspheric lens, a 300 lines/mm grating, and a 512 pixel InGaAs array detector (Hamamatsu, 900−1700 nm) were used for signal detection. The typical integration time for PL measurements is 30 s.

Results and Discussion

CD spectra for LYZ-SWNT dispersions at different concentrations of GndHCl are presented in Figure 2a. The CD band at 200−260 nm can be used to calculate the percentage of denatured lysozyme.[22] The calculated percentage of denatured lysozyme obtained from the CD intensity at 220 nm is plotted against the concentration of GndHCl (Figure 2b), which shows that lysozyme in LYZ-SWNT begins to irreversibly denature at ∼4.5 M GndHCl. This concentration is higher than that for free-state lysozyme (2.5 M[23]).

Figure 3a,b shows Raman spectra of the LYZ-SWNT dispersion at different GndHCl concentrations. At 532 nm excitation (Figure 3a), Raman bands are assigned to the (9,3) nanotube (metallic) according to the observed resonant excitation.[24] At 647 nm excitation, the radial breathing modes (RBM) at 283 and 298 cm^{-1} can be assigned to two semiconducting nanotubes: (7,5) and (8,3),[11,24] respectively. Frequencies of the G bands (∼1590 cm^{-1}) and G' bands (∼2600 cm^{-1}) did not shift at either the 532 nm or the 647 nm excitation. This observation is consistent with the hypothesis of a pure hydrophobic interaction between the protein and nanotubes. Because lysozyme does not contain a metallic center, no doping level changes or charge transfer is expected between lysozyme and SWNTs during the lysozyme denaturation process.[25−27]

The structural change of lysozyme during denaturation may change the conformation of the LYZ-SWNT complex, which results in changing the surroundings of SWNTs and then changing the E_{ii} of SWNTs,[7,28] hence changing their Raman intensity. However, it is difficult to track the absolute Raman intensity changes for a certain Raman peak because the over-

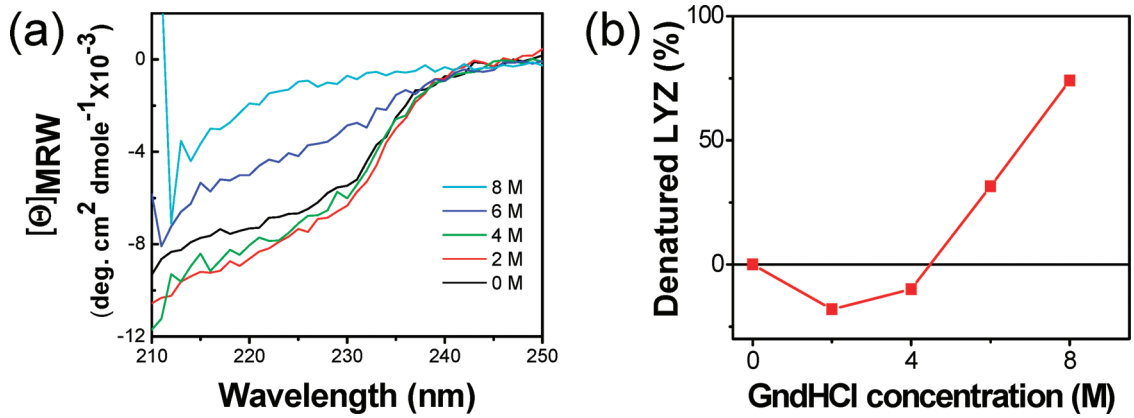

Figure 2. (a) Circular dichroism spectra of lysozyme at different GndHCl concentrations. Here, Θ_{MRW} denotes the ellipticity in the mean residue weight. (b) A denaturation plot shown for LYZ-SWNT. The percent denatured lysozyme is calculated from the ellipticity at 222 nm shown in (a).

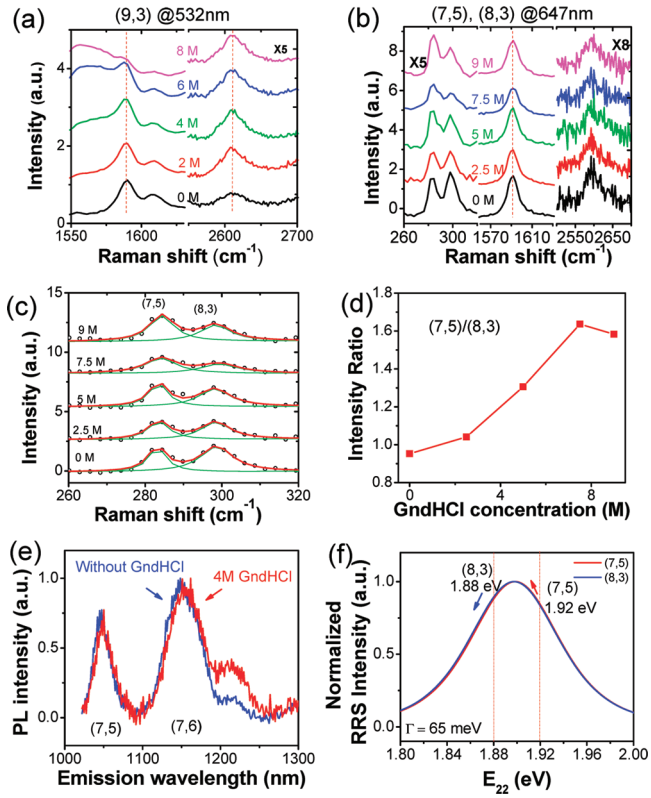

Figure 3. Raman spectra of the lysozyme−SWNT dispersion with different GndHCl concentrations: (a) at 532 nm excitation for (9,3) SWNTs and (b) at 647 nm excitation for (7,5) and (8,3) SWNTs. (c) Lorentzian fits of RBM bands of (7,5) and (8,3) nanotubes at different GndHCl concentrations. (d) Plot of the RBM integrated intensity ratio ($I_{(7,5)}/I_{(8,3)}$) for the (7,5) to (8,3) nanotubes vs the GndHCl concentration. (e) PL of the LYZ-SWNT dispersion without any GndHCl (blue line) and with 4 M GndHCl (red line). The excitation wavelength is 658 nm. Emission intensity is normalized at the emission peaks occurring around 1150 nm. (f) Calculated normalized intensity of the Stokes RBM bands for (7,5) (red line) and (8,3) (blue line) at 647 nm (1.916 eV) laser excitation as a function of E_{22}, and the fwhm resonance window width of 65 meV is indicated.

all intensity also changes as a function of the experimental conditions, such as laser focus, refractive index of the solution, and the concentration of SWNTs. In our experiments, the RBM intensity ratio of the 283 cm^{-1} peak ((7,5) nanotube) to the 298 cm^{-1} peak ((8,3) nanotube) at 647 nm excitation changed during lysozyme denaturation (Figure 3b). Both (7,5) and (8,3) nanotubes belong to the same ($2n + m = 19$) family for semiconducting nanotubes, which means that the two species have similar diameters but different chiral angles. To quantify the changes of the RBM intensity ratio, the observed RBM bands for the (7,5) and (8,3) nanotubes were fit by two Lorentzian peaks (Figure 3c). The RBM intensity ratio ($I_{(7,5)}/I_{(8,3)}$) for the (7,5) to (8,3) tubes is then plotted against the concentration of GndHCl (Figure 3d), which shows that the ratio increases significantly for GndHCl concentrations higher than 4 M. This intensity ratio change can be correlated with the denaturation curve of the LYZ−SWNT in Figure 2b and suggests that the RBM intensity ratio $I_{(7,5)}/I_{(8,3)}$ can also be used to indicate lysozyme denaturation.

The change observed in $I_{(7,5)}/I_{(8,3)}$ is attributed to the E_{ii} shift of SWNTs during lysozyme denaturation. To validate this shift, PL measurements were carried out (Figure 3e). The PL emission peaks around 1050 and 1150 nm are assigned to (7,5) and (7,6) nanotubes, respectively.[24,29] After adding 4 M GndHCl, emission peaks from the (7,5) and (7,6) nanotubes exhibit a red shift of

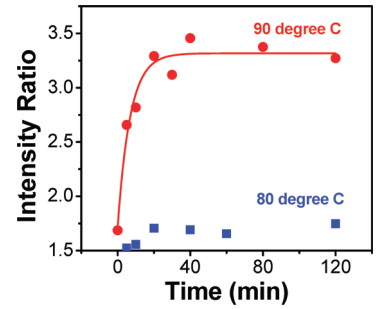

Figure 4. Plot of the RBM intensity ratio $I_{(7,5)}/I_{(8,3)}$ of (7,5) to (8,3) nanotubes as a function of heating time at 80 °C (blue solid squares) and 90 °C (red solid circles). The red line is an exponential-decay fit ($y = A^*\exp(-kx) + B$) for data taken at 90 °C, and the rate constant $k = 0.15$ min^{-1} is obtained for data at 90 °C.

~3 and ~5 meV, respectively. These relatively small red shifts indicate that SWNTs are surrounded by material with a larger dielectric constant after lysozyme denaturation. We also note that, even at GdnHCl concentrations lower than 4M, the intensity ratio increases, while the CD spectrum shows an opposite change (Figure 3).

We explain the observed Raman intensity ratio changes based on resonance Raman theory. The resonance Raman intensity of SWNTs can be expressed by the following expression[30]

$$I_{\text{Stokes}} \propto \left| \frac{1}{(E_{\text{laser}} - E_{ii} - i\Gamma)(E_{\text{laser}} + E_{\text{ph}} - E_{ii} - i\Gamma)} \right|^2$$

where E_{laser} is the laser energy, E_{ph} is the phonon energy, i is the imaginary unit, and Γ is the width of the resonance window. In writing this expression for I_{Stokes}, the matrix elements for optical absorption, electron−phonon interaction, and optical emission are considered to be constant. For all mod [$(n - m)$, 3] = 2 SWNTs, a red shift occurs for both E_{22} and E_{11} when the SWNTs are surrounded by materials having a dielectric constant larger than unity.[31] Therefore, the E_{22} level for (7,5) and (8,3) nanotubes is red shifted during the denaturation of lysozyme. The E_{22} values for (7,5) and (8,3) nanotubes are around 1.92 and 1.88 eV, respectively.[24,29] Figure 3f shows a plot of resonance Raman intensity versus E_{22} (65 meV is used for Γ,[30] where $E_{\text{laser}} = 1.916$ eV (647 nm)). The plots for the normalized RBM intensity versus E_{22} for the (7,5) and (8,3) nanotubes almost overlap with each other because their RBM frequencies are close to each other. Assuming that the E_{22} shift is small (<20 meV), then as the E_{22} transitions red shift, the RBM intensity for the (7,5) nanotubes should increase and the RBM intensity of the (8,3) nanotube should decrease (Figure 3f). As a result, the RBM intensity ratio for (7,5) to (8,3) should increase, which is in good agreement with the experimental results (Figure 3d).

To confirm our results and to eliminate any spectral artifacts that might be introduced by the chemical denaturant used in this experiment, thermal denaturation of LYZ-SWNT was carried out. The denaturation of lysozyme under elevated temperature has been studied extensively before.[32] In this experiment, the denaturation of lysozyme was conducted at 80 and 90 °C. A similar change in the Raman results was observed: the G band and G′ band peaks did not shift (not shown), but the RBM intensity ratio of (7,5) to (8,3) ($I_{(7,5)}/I_{(8,3)}$) increased during the thermal denaturation (Figure 4). At 90 °C, the RBM intensity ratio increased rapidly within the first 10 min and then approached a maximum value of ~3.2. The maximum value of

the RBM intensity ratio suggests the complete denaturation of lysozyme in the LYZ-SWNT dispersion. Assuming that the RBM intensity change is proportional to the denatured lysozyme, the first-order rate constant k for the thermal denaturation of lysozyme can be obtained by fitting the time-dependent RBM intensity ratio by an exponential function, $I = A^*\exp(-kt) + B$, where I is the RBM intensity ratio, t is the denaturation time, k is the rate constant, and A and B are constants. The fit result gives a k value of 0.15 ± 0.02 min^{-1} at 90 °C, which is lower than that for free lysozyme ($\sim$1.2 min^{-1} estimated for 3×10^{-4} M lysozyme at pH = 6.2[33]). The smaller rate constant of denaturation indicates that nanotube-bound lysozyme may be more thermally stable. At 80 °C, the RBM intensity ratio increases slowly, also indicating a lower rate constant. More systematic thermal studies will be required to elucidate the detailed thermally induced degradation kinetics for proteins in the protein-bound nanotube system.

Conclusion

In conclusion, Raman and PL measurements have been done on LYZ-SWNT dispersions during the denaturation of lysozyme. Intensity changes in the Raman peaks and a red shift of the PL emission have been observed, which are correlated with the denaturation curves for lysozyme obtained from the CD spectra. By using lysozyme as a model protein, our results show that SWNTs can potentially be used as an optical probe to monitor the denaturation of small proteins. The scientific principles could potentially be applied to other SWNT−protein hybrid systems, such as nanotube-based sensor devices.

Acknowledgment. This work was supported by the Pfizer-MIT Strategic Alliance. L.M.X. acknowledges a Scholarship from the China Scholarship Council, the Peking University CDY Scholarship, and the NSFC (20725307 and 20808004). M.S.D. gratefully acknowledges support from the NSF DMR 07-04197.

References and Notes

(1) Schellekens, H. *Nat. Rev. Drug Discovery* **2002**, *1*, 457.
(2) Tessier, P. M.; Jinkoji, J.; Cheng, Y. C.; Prentice, J. L.; Lenhoff, A. M. *J. Am. Chem. Soc.* **2008**, *130*, 3106.
(3) Saito, R.; Dresselhaus, G.; Dresselhaus, M. S. *Physical Properties of Carbon Nanotubes*; Imperial College Press: London, U.K., 1998.
(4) Jorio, A., Dresselhaus, G., Dresselhaus, M. S., Eds. *Carbon Nanotubes*; Topics in Applied Physics; Springer-Verlag: Berlin, 2008; Vol. 111.
(5) Mintmire, J. W.; White, C. T. *Phys. Rev. Lett.* **1998**, *81*, 2506.
(6) Saito, R.; Dresselhaus, G.; Dresselhaus, M. S. *Phys. Rev. B* **2000**, *61*, 2981.
(7) Miyauchi, Y.; Saito, R.; Sato, K.; Ohno, Y.; Iwasaki, S.; Mizutani, T.; Jiang, J.; Maruyama, S. *Chem. Phys. Lett.* **2007**, *442*, 394.
(8) Araujo, P. T.; Doorn, S. K.; Kilina, S.; Tretiak, S.; Einarsson, E.; Maruyama, S.; Chacham, H.; Pimenta, M. A.; Jorio, A. *Phys. Rev. Lett.* **2007**, *98*, 067401.
(9) Heller, D. A.; Baik, S.; Eurell, T. E.; Strano, M. S. *Adv. Mater.* **2005**, *17*, 2793.
(10) Liu, Z.; Davis, C.; Cai, W. B.; He, L.; Chen, X. Y.; Dai, H. J. *Proc. Natl. Acad. Sci. U.S.A.* **2008**, *105*, 1410.
(11) Heller, D. A.; Jeng, E. S.; Yeung, T. K.; Martinez, B. M.; Moll, A. E.; Gastala, J. B.; Strano, M. S. *Science* **2006**, *311*, 508.
(12) Jeng, E. S.; Moll, A. E.; Roy, A. C.; Gastala, J. B.; Strano, M. S. *Nano Lett.* **2006**, *6*, 371.
(13) Souza, A. G.; Kobayashi, N.; Jiang, J.; Grüneis, A.; Saito, R.; Cronin, S. B.; Mendes, J.; Samsonidze, G. G.; Dresselhaus, G. G.; Dresselhaus, M. S. *Phys. Rev. Lett.* **2005**, *95*, 217403.
(14) Dresselhaus, M. S.; Dresselhaus, G.; Jorio, A.; Souza, A. G.; Pimenta, M. A.; Saito, R. *Acc. Chem. Res.* **2002**, *35*, 1070.
(15) Duan, X. J.; Son, H. B.; Gao, B.; Zhang, J.; Wu, T. J.; Samsonidze, G. G.; Dresselhaus, M. S.; Liu, Z. F.; Kong, J. *Nano Lett.* **2007**, *7*, 2116.
(16) Nepal, D.; Geckeler, K. E. *Small* **2006**, *2*, 406.
(17) Matsuura, K.; Saito, T.; Okazaki, T.; Ohshima, S.; Yumura, M.; Iijima, S. *Chem. Phys. Lett.* **2006**, *429*, 497.
(18) Cao, J.; Pham, D. K.; Tonge, L.; Nicolau, D. V. *Smart Mater. Struct.* **2002**, *11*, 772.
(19) Blake, C. C. F.; Koenig, D. F.; Mair, G. A.; North, A. C. T.; Phillips, D. C.; Sarma, V. R. *Nature* **1965**, *206*, 757.
(20) Kepka, A. G.; Grossweiner, L. I. *Photochem. Photobiol.* **1973**, *18*, 49.
(21) Baugher, J. F.; Grossweiner, L. I.; Lewis, C. *J. Chem. Soc., Faraday Trans. 2* **1974**, *70*, 1389.
(22) Knubovets, T.; Osterhout, J. J.; Connolly, P. J.; Klibanov, A. M. *Proc. Natl. Acad. Sci. U.S.A.* **1999**, *96*, 1262.
(23) Greene, R. F., Jr.; Pace, C. N. *J. Biol. Chem.* **1974**, *249*, 5388.
(24) Jorio, A.; Santos, A. P.; Ribeiro, H. B.; Fantini, C.; Souza, M.; Vieira, J. P. M.; Furtado, C. A.; Jiang, J.; Saito, R.; Balzano, L.; Resasco, D. E.; Pimenta, M. A. *Phys. Rev. B* **2005**, *72*, 075207.
(25) Rao, A. M.; Eklund, P. C.; Bandow, S.; Thess, A.; Smalley, R. E. *Nature* **1997**, *388*, 257.
(26) Shim, M.; Ozel, T.; Gaur, A.; Wang, C. J. *J. Am. Chem. Soc.* **2006**, *128*, 7522.
(27) Maciel, I. O.; Anderson, N.; Pimenta, M. A.; Hartschuh, A.; Qian, H.; Terrones, M.; Terrones, H.; Campos-Delgado, J.; Rao, A. M.; Novotny, L.; Jorio, A. *Nat. Mater.* **2008**, *7*, 878.
(28) Choi, J. H.; Strano, M. S. *Appl. Phys. Lett.* **2007**, *90*, 223114.
(29) Bachilo, S. M.; Strano, M. S.; Kittrell, C.; Hauge, R. H.; Smalley, R. E.; Weisman, R. B. *Science* **2002**, *298*, 2361.
(30) Fantini, C.; Jorio, A.; Souza, M.; Strano, M. S.; Dresselhaus, M. S.; Pimenta, M. A. *Phys. Rev. Lett.* **2004**, *93*, 147406.
(31) Ohno, Y.; Iwasaki, S.; Murakami, Y.; Kishimoto, S.; Maruyama, S.; Mizutani, T. *Phys. Rev. B* **2006**, *73*, 235427.
(32) Morozova, L.; Haezebrouck, P.; Vancauwelaert, F. *Biophys. Chem.* **1991**, *41*, 185.
(33) Nohara, D.; Mizutani, A.; Sakai, T. *J. Biosci. Bioeng.* **1999**, *87*, 199.

JP9121497